Inverse Aerodynamic Optimization Considering Impacts of Design Tip Speed Ratio for Variable-Speed Wind Turbines

Zhiqiang Yang [1], Minghui Yin [1,*], Yan Xu [2], Yun Zou [1], Zhao Yang Dong [3,4] and Qian Zhou [5]

[1]   School of Automation, Nanjing University of Science and Technology, Nanjing 210094, China;
      yang-zhiqiang@foxmail.com (Z.Y.); zouyun@vip.163.com (Y.Z.)
[2]   School of Electrical and Electronic Engineering, Nanyang Technological University, Singapore 639798,
      Singapore; eeyanxu@gmail.com
[3]   China Southern Power Grid Electric Power Research Institute, Guangzhou 510000, China; zydong@ieee.org
[4]   School of Electrical and Information Engineering, University of Sydney, Sydney, NSW 2006, Australia
[5]   Jiangsu Electric Power Company Research Institute, Nanjing 211103, China; xjtu@163.com
[*] Correspondence: ymhui@vip.163.com; Tel.: +86-151-0516-8909

Abstract: Because of the slow dynamic behavior of the large-inertia wind turbine rotor, variable-speed wind turbines (VSWTs) are actually unable to keep operating at the design tip speed ratio (TSR) during the maximum power point tracking (MPPT) process. Moreover, it has been pointed out that although a larger design TSR can increase the maximum power coefficient, it also greatly prolongs the MPPT process of VSWTs. Consequently, turbines spend more time operating at the off-design TSRs and the wind energy capture efficiency is decreased. Therefore, in the inverse aerodynamic design of VSWTs, the static aerodynamic performance (i.e., the maximum power coefficient) and the dynamic process of MPPT should be comprehensively modeled for determining an appropriate design TSR. In this paper, based on the inverse design method, an aerodynamic optimization method for VSWTs, fully considering the impacts of the design TSR on the static and dynamic behavior of wind turbines is proposed. In this method, to achieve higher wind energy production, the design TSR, chord length and twist angle are jointly optimized, which is structurally different from the conventional separated design procedure. Finally, the effectiveness of the proposed method is validated by simulation results based on the Bladed software.

Keywords: aerodynamic optimization; design tip speed ratio (TSR); maximum power point tracking (MPPT); inverse design; variable-speed wind turbine (VSWT)

1. Introduction

Wind energy has been receiving increasing attention as one of the most exploitable renewable energy sources. The efficiency of wind energy conversion is mainly dependent on the aerodynamic shape of the wind turbine rotor [1], an essential component of a wind turbine for harvesting wind energy. Therefore, the aerodynamic optimization of wind turbine rotors plays a crucial role in the design of wind turbines. Generally, the current aerodynamic design for wind turbines is divided into two major categories: the direct method [2–10] and the inverse method [11–17]. As compared with the former, the latter is distinguished by its clear principle, analytical process and fast convergence. In the inverse method, some basic design parameters (e.g., design tip speed ratio, blade number, blade radius, hub radius and airfoil distribution) and the desired aerodynamic characteristic (e.g., peak power, rated wind speed and lift coefficient distribution) are firstly specified. Then, the aerodynamic shape parameters (e.g., the blade chord and twist distributions) are directly obtained via analytical calculation.

Variable-speed wind turbines (VSWTs) have become the mainstream of large-scale wind power generation systems in recent years [18,19]. They mostly operate in the variable-speed region [20], which corresponds to the wind speed range from the cut-in to the rated speed. In this region, the maximum power point tracking (MPPT) control is employed to regulate rotor speed according to wind speed variation so that the VSWT can be maintained at the design tip speed ratio (TSR) λ_{dgn} (also called the optimal TSR λ_{opt}) [21]. Therefore, in the conventional inverse methods for the aerodynamic optimization of VSWTs, such as the Glauert method [11], the Wilson method [12] and others [13–17] based on the blade element momentum (BEM) theory, the primary objective is to maximize the power coefficient at a specified λ_{dgn}.

As one of the basic parameters in the inverse methods for the aerodynamic optimization of VSWTs, λ_{dgn} exerts a considerable influence upon the aerodynamic shape of rotors [22,23], including the radial chord and twist distributions. To obtain an appropriate λ_{dgn}, the functional relation between λ_{dgn} and the maximum power coefficient $C_{p,max}$, which is regarded as a type of the turbines' static aerodynamic performance, has been discussed in References [24–27]. According to this relation, the λ_{dgn} corresponding to the maximum value of $C_{p,max}$ is selected and then the chord and twist distributions are optimized based on this λ_{dgn} by an inverse method in Reference [13].

Obviously, in the aforementioned inverse methods, λ_{dgn} is determined only based on the static aerodynamic performance, and the impact of λ_{dgn} on the dynamic process of MPPT is usually neglected. This may result in a considerable reduction in VSWTs' efficiency, as interpreted below:

(1) The wind energy capture efficiency, as a closed-loop performance of VSWTs, is actually dependent on not only the static aerodynamic performance but also the MPPT dynamics. It has been pointed out in References [10,28–31] that turbines with large inertia usually track λ_{dgn} rather than maintaining at λ_{dgn}. Moreover, the longer the dynamic process lasts, the lower the wind energy capture efficiency is. Especially for the VSWTs designed for low wind speed regions, larger inertia of the wind turbine rotor and weaker aerodynamic torque result in a slower dynamic behavior and a longer dynamic process of MPPT. Therefore, the dynamic process of MPPT and its effect on the wind energy production should be carefully modeled, especially for the low wind speed VSWTs.

(2) Besides $C_{p,max}$, λ_{dgn} also has an effect on the dynamic process of MPPT. With the decrease (increase) of λ_{dgn}, the MPPT process is shortened (lengthened) and correspondingly the wind energy capture efficiency is increased (decreased) [32].

(3) To sum up, λ_{dgn} exerts a comprehensive influence upon the wind energy capture efficiency through the static aerodynamic performance and the MPPT dynamics. If a larger λ_{dgn} is conventionally applied just for improving the static aerodynamic performance (i.e., $C_{p,max}$), the turbine has to spend more time operating at the off-design TSRs due to the prolonged dynamic process of MPPT and eventually the overall efficiency of the closed-loop VSWT system is reduced.

Therefore, in the inverse aerodynamic design of VSWT rotors, the static aerodynamic performance and the dynamic process of MPPT should be compromised for determining an appropriate λ_{dgn}. In this paper, based on the inverse design program PROPID [33,34] for the aerodynamic optimization of VSWTs, an inverse method fully considering the impact of λ_{dgn} on the static and dynamic behavior of turbines is proposed. Compared to the existing separated design procedure, λ_{dgn}, chord length and twist angle are jointly optimized to maximize the closed-loop performance of VSWTs (i.e., wind energy capture efficiency) in this method. Finally, the proposed method is verified by the simulation results based on the commercial software Bladed [35,36].

2. Problem Description

Actually, the wind energy capture efficiency, as a closed-loop performance of VSWTs, is collectively determined by the static aerodynamic performance as well as the MPPT dynamics. Although a larger

design TSR can contribute to better static aerodynamic performance (i.e., higher $C_{p,max}$), it also greatly increases the duration of the dynamic process of MPPT so that the overall efficiency of the closed-loop VSWT system can be reduced. However, this comprehensive impact of λ_{dgn} on wind energy capture efficiency through static aerodynamic performance and MPPT dynamics is usually ignored by the conventional aerodynamic design of VSWTs in the literature.

2.1. Relationship between λ_{dgn} and $C_{p,max}$

For single-airfoil wind turbine rotors, the relationship between λ_{dgn} and $C_{p,max}$ characterized by a parabolic function has been derived in References [24–26]. Furthermore, for multi-airfoil wind turbine rotors, which are generally implemented in practical VSWTs, the 1.5 MW wind partnership for advanced component technologies (WindPACT) turbine [37] developed by the national renewable energy laboratory (NREL), is chosen for analyzing the relation of $C_{p,max}$ with λ_{dgn}. Specifically, keeping the original blade radius, hub radius and airfoils unchanged, the PROPID code [33,34] is applied to design the aerodynamic shape of the WindPACT turbine according to the different λ_{dgn}, which ranges from 5.0 to 10.0 with a step size of 0.5. Then, $C_{p,max}$ of the redesigned wind turbine rotors corresponding to an array of λ_{dgn} are respectively calculated by the software Bladed.

As shown in Figure 1, the variation of $C_{p,max}$ versus λ_{dgn} also exhibits a parabolic shape and the maximum value of $C_{p,max}$ occurs at λ_{dgn} = 8.5. Therefore, λ_{dgn} corresponding to the maximum value of $C_{p,max}$ is selected in the existing inverse methods [11–15].
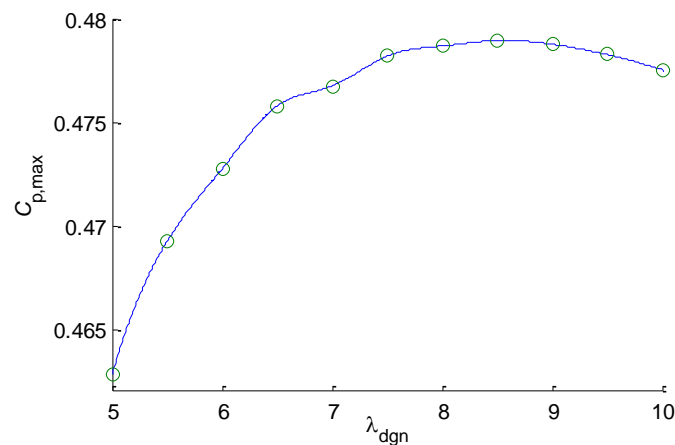

Figure 1. The variation of $C_{p,max}$ versus λ_{dgn} obtained from simulations on the WindPACT turbine.

2.2. The Impact of λ_{dgn} on the Maximum Power Point Tracking (MPPT) Process

Besides the aforementioned $C_{p,max}$, it has been shown from the viewpoint of a closed-loop model of VSWTs that λ_{dgn} has a significant impact on the dynamic process of MPPT [32].

2.2.1. A Closed-Loop Model of Variable-Speed Wind Turbines (VSWTs)

As shown in Figure 2, a closed-loop model of VSWTs consists of turbulent wind, a wind turbine rotor, a drive train, a generator and a MPPT controller. Note that because the electromagnetic response is much faster than the mechanical one, the converter can be neglected and the generator is assumed to instantly follow the torque reference requested by the MPPT controller [30].
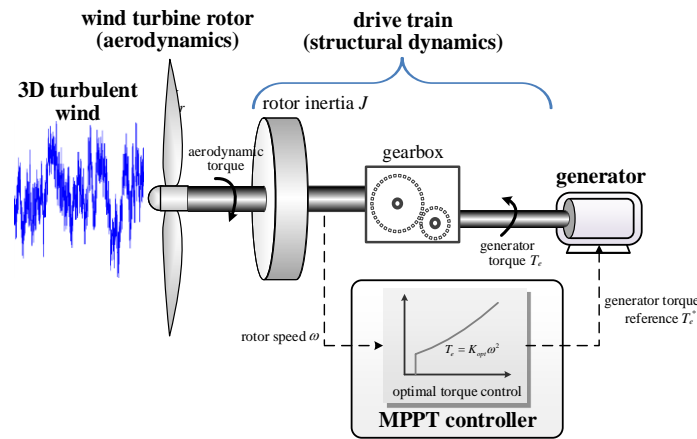
Figure 2. A closed-loop model of variable-speed wind turbines (VSWTs).

In this paper, the commercial software Bladed [35,36] is employed to conduct the time-domain dynamic simulation of the closed-loop model. This software has passed the Germanischer Lloyd's certification and has been widely applied for wind turbine design, analysis and validation.

The aerodynamic model used within Bladed is based on the BEM theory. To sufficiently reproduce the dynamics of rotor wake and induced velocity flow field (i.e., the vorticity trailed into the rotor wake is influenced by the change in blade loading and the time for the change of the induced flow field is finite), the dynamic inflow model [35] is selected.

The commonly-used control strategy for MPPT, known as the optimal torque (OT) control [38], is employed. To track maximum power point, the OT control regulates the generator torque according to the measured rotor speed and a predefined torque versus rotor speed curve that is expressed as:

$$T_e = K_{opt}\omega^2, \ K_{opt} = 0.5\rho\pi R^5 C_{p,max}/\lambda_{opt}^3, \tag{1}$$

where ω is the rotor speed, ρ is the air density, R is the blade length and λ_{opt} is equal to λ_{dgn}.

2.2.2. The Impact of λ_{dgn} on the MPPT Process

The optimal rotor speed ω_{opt} for MPPT is defined as

$$\omega_{opt} = \lambda_{dgn}v/R \tag{2}$$

where v is the wind speed. The tracking range of rotor speed, defined as the difference of ω_{opt} corresponding to wind speed variation, is proportionally related to λ_{dgn}. Obviously, λ_{dgn} exerts a direct influence upon the dynamic process of MPPT.

To illustrate the impact of λ_{dgn} on the MPPT process, simulations on the redesigned WindPACT turbines with two different λ_{dgn} (i.e., 5.5 and 8.5) excited by a step variation of wind speed are conducted by the Bladed software. The simulation results are compared in Figure 3 and Table 1, respectively. It can be seen that as λ_{dgn} increases, the tracking range of rotor speed is widened, which results in a longer dynamic process of MPPT. Correspondingly, the rotor spends more time operating at the off-design TSRs.
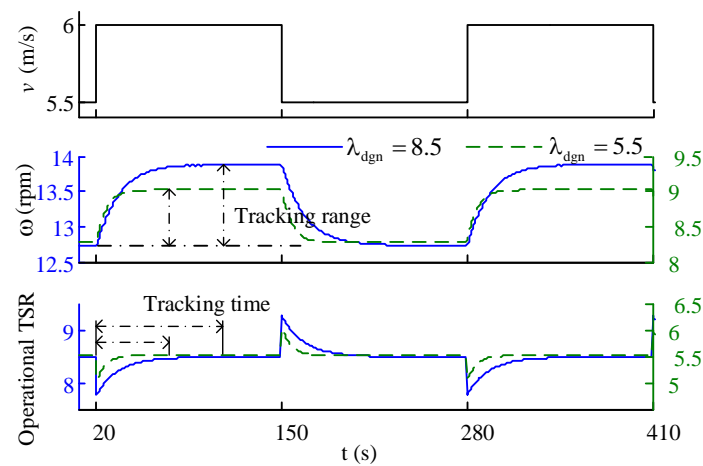
Figure 3. Trajectories of the wind turbines with different λ_{dgn} excited by a same step wind speed.

Table 1. Response of the wind turbines with different λ_{dgn} excited by a same step wind speed.

λ_{dgn}	5.5	8.5
Tracking range (rpm)	0.7517	1.1535
Tacking time (s)	66.8	100.0

Furthermore, for a given turbulent wind (mean wind speed is 6.5 m/s and the turbulence class is *A* [39]), the probability distributions of operational TSR corresponding to an array of λ_{dgn} (from 5.0 to 10.0) are obtained by the dynamic simulations and plotted in Figure 4. It also can be observed that the larger the λ_{dgn}, the smaller the probability of operational TSR around λ_{dgn}, namely, the more time the turbine will take to operate at the off-design TSRs.
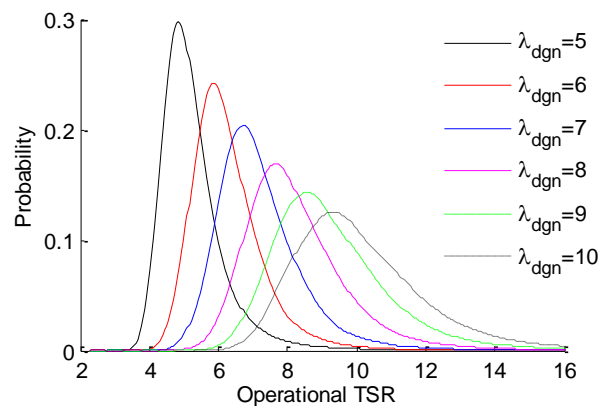

Figure 4. The probability distribution of operational tip speed ratio (TSR) corresponding to an array of λ_{dgn}.

2.3. The Comprehensive Impact of λ_{dgn} on Wind Energy Capture Efficiency via $C_{p,max}$ and the MPPT Process

Because off-design TSRs correspond to the power coefficients less than $C_{p,max}$, running at such TSRs results in tracking losses [28–31]. It is inferred that if a turbine operates at off-design TSRs for a long duration due to the increasing of λ_{dgn}, its MPPT efficiency is inevitably reduced. Therefore, by combining the discussion mentioned in Sections 2.1 and 2.2, λ_{dgn} actually exerts a comprehensive impact on the wind energy production of VSWTs through static aerodynamic performance and MPPT dynamics. That is to say, although a relatively large λ_{dgn} yielding the maximum value of $C_{p,max}$ can

contribute to improving the wind energy capture efficiency, the overall efficiency is probably reduced due to the long-duration dynamic process of MPPT.

To demonstrate such a comprehensive impact of λ_{dgn} on wind energy capture efficiency, the relationship between the efficiency and λ_{dgn} is obtained via the Bladed-based simulation on the WindPACT turbine. Note that the wind energy capture efficiency P_{favg} [20] is in fact a closed-loop performance indicator of VSWTs operating under turbulent wind. Its expression and calculation are provided in Section 3.1. As depicted in Figure 5, P_{favg} first increases and then decreases with λ_{dgn}. This indicates that with the increase of λ_{dgn}, the prolonged MPPT process rather than the raised $C_{p,max}$ gradually plays a dominant role in the MPPT performance.
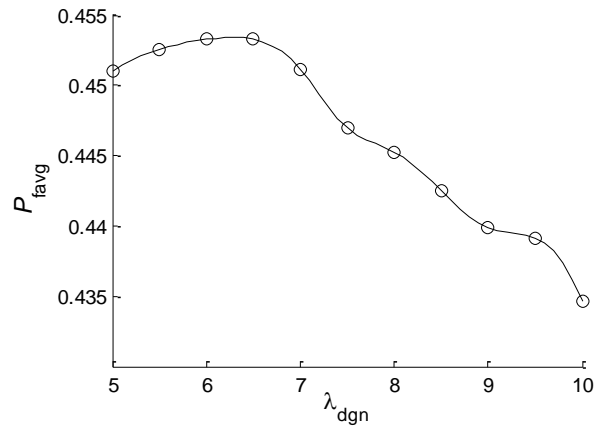

Figure 5. The relationship between P_{favg} and λ_{dgn}.

Hence, there is a tradeoff, which can be optimized by λ_{dgn}, between the static aerodynamic performance (i.e., increasing $C_{p,max}$) and the dynamic process of MPPT (i.e., reducing the tracking range of rotor speed). They should be simultaneously considered in determining λ_{dgn} so that the wind energy capture efficiency can be eventually improved.

3. Aerodynamic Optimization Considering the Comprehensive Impact of $\lambda_{\mathbf{dgn}}$

Based on the inverse design method, this paper proposes a new method for the aerodynamic optimization of VSWTs. Different from the separated procedure applied in the conventional methods, the design TSR and the distributions of chord and twist are jointly optimized for maximizing the wind energy capture efficiency in the proposed method so that the effect of λ_{dgn} on both $C_{p,max}$ and the MPPT process can be integrally considered. Essentially, the new method aims to improve the closed-loop performance of VSWTs through the coordination between the static aerodynamic performance and the MPPT dynamics.

3.1. Wind Energy Capture Efficiency

The wind energy capture efficiency is approximated as the ratio of the captured power to the available wind power P_{favg} [20], i.e.,

$$
\begin{aligned}
P_{favg} &= \frac{1}{N}\sum_{i=1}^{N} P_{cap}^{i} \Big/ \frac{1}{N}\sum_{i=1}^{N} P_{inflow}^{i} \\
P_{cap}^{i} &= T_{e,i}\omega_{e,i} + J\omega_{i}\dot{\omega}_{i} \\
P_{inflow}^{i} &= 0.5\rho\pi R^{2}v_{i}^{3}
\end{aligned}
\tag{3}
$$

where N is the total of the simulation steps, J is the rotor inertia, v_i, P_{cap}^{i}, P_{inflow}^{i}, ω_i, $T_{e,i}$ and $\omega_{e,i}$ are the wind speed, captured wind power, inflow wind power, rotor speed, generator torque and generator speed at the i-th step, respectively.

Before calculating P_{favg} according to the Equation (3), the dynamic simulation on the closed-loop model of VSWTs is conducted for a given turbulent wind. The detailed procedure for calculating P_{favg} is described as follows:

Step 1 Model the concerning wind turbine in the Bladed software, including wind turbine rotor, drive train, tower, and etc.
Step 2 Call the aerodynamic analysis module provided by the Bladed software to calculate the rotor's optimal TSR λ_{opt} and the corresponding maximum power coefficient $C_{\text{p,max}}$.
Step 3 Configure the parameters of the MPPT controller by the Equation (1).
Step 4 Perform the dynamic simulation module in the Bladed software with the given turbulent wind and obtain the simulated trajectories of the wind turbine.
Step 5 Calculate P_{favg} according to the Equation (3) based on the simulated trajectories.

3.2. Joint Aerodynamic Optimization Based on the Inverse Design

The schematic diagrams of the conventional inverse design and the joint aerodynamic optimization proposed in this paper are illustrated in Figure 6. In the former method, as shown in Figure 6a, λ_{dgn} is first determined according to the relationship between λ_{dgn} and $C_{\text{p,max}}$, then the aerodynamic shape is derived through analytical calculation for the specified λ_{dgn} and other basic parameters (e.g., hub radius, rotor radius and airfoil distribution). Obviously, λ_{dgn} and the aerodynamic shape are separately obtained and the comprehensive effect of λ_{dgn} on the wind energy capture efficiency cannot be considered. To overcome this disadvantage, this paper proposes a new aerodynamic optimization method based on the inverse design. In this method, as represented in Figure 6b, by introducing P_{favg} as a performance indicator, λ_{dgn} and the aerodynamic shape are jointly optimized so that the static aerodynamic performance and the MPPT dynamics, which are dependent on λ_{dgn}, are coordinated.
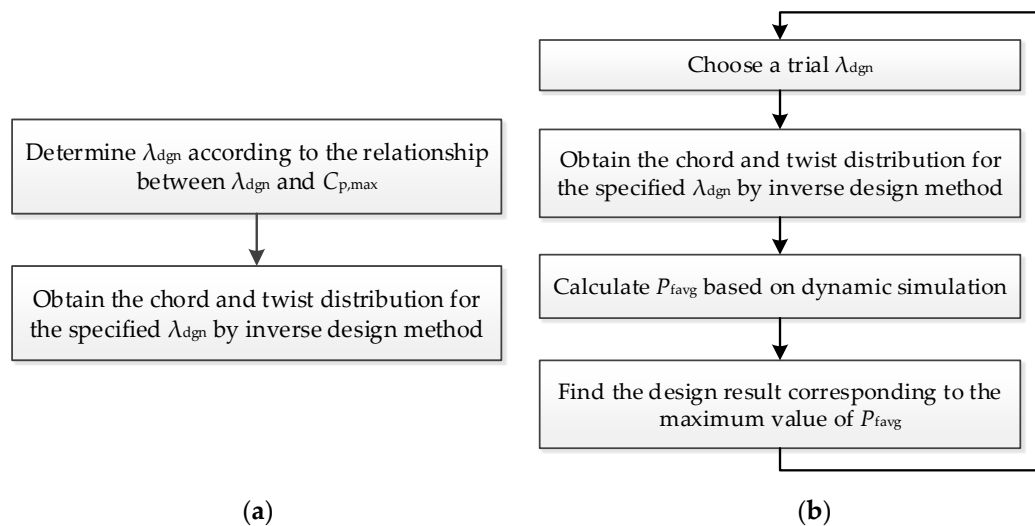

Figure 6. The schematic diagrams of the conventional inverse design and the proposed aerodynamic design. (**a**) Separated optimization in the inverse design method; (**b**) Joint optimization in the proposed method.

Specifically, in the proposed method, the PROPID code [32,33] is employed for inverse aerodynamic design; P_{favg} is calculated based on the Bladed-based dynamic simulation; the interval quartering algorithm [40] is adopted to search the aerodynamic design with maximum P_{favg} from a number of trial λ_{dgn}. The flowchart of the joint aerodynamic optimization for VSWTs is shown in Figure 7 and the detailed procedure is described as follows:

Step 1 Initialization.

> **Step 1.1** Initialize the aerodynamic parameters according to the baseline wind turbine, including blade number B, blade length R, rotor hub radius R_{hub}, airfoils and original distributions of chord and twist. B, R, R_{hub} and airfoils (including the relative thickness) remain unchanged during the optimization procedure.
>
> **Step 1.2** Initialize the PROPID code with B, R, R_{hub}, airfoils and original distributions of chord and twist determined in Step 1.1.
>
> **Step 1.3** Considering the constraints of material cost and noise, λ_{dgn} usually ranges from 5.0 to 9.0 [22,23]. Thus, set the search interval of λ_{dgn} as [5.0, 9.0] in this paper.

Step 2 Divide the search interval equally into four connected subintervals and generate three independent boundaries of all the subintervals.

Step 3 Choose one of the boundaries as a trial λ_{dgn}.

Step 4 Call the PROPID code to perform the inverse design for the chosen λ_{dgn} and obtain the aerodynamic shape parameters.

> **Step 4.1** Specify the distributions of lift coefficient and axial induction factor. It is assumed that the lift coefficient distributes around the maximum lift-to-drag ratio of airfoils along the blade span, as listed in Appendix A, and the axial induction factor of each blade section is 0.333, except the sections near the blade root [33].
>
> **Step 4.2** Run the PROPID code to derive the distributions of chord and twist corresponding to the chosen λ_{dgn}. Thus, a newly designed wind turbine with the λ_{dgn} chosen at Step 3 is obtained.

Step 5 Calculate P_{favg} for the newly designed turbine according to the procedure presented in Section 3.1.

Step 6 Check whether all the three boundaries are chosen. If yes, go to Step 7; otherwise, return to Step 3.

Step 7 Check whether the length of the subinterval is less than a termination threshold (which is determined as 0.1 in this paper by comprehensively considering the optimization result and the manufacturing precision of wind turbine blades). If yes, go to Step 8; otherwise, define the two adjacent subintervals sharing the boundary corresponding to the maximum P_{favg} as the new search interval, and then go to Step 2.

Step 8 Output the jointly optimized wind turbine rotor corresponding to the maximum P_{favg}.
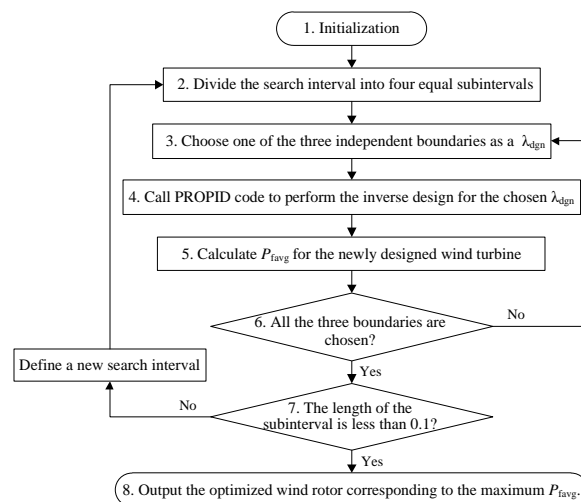

Figure 7. Flowchart of the aerodynamic optimization of the VSWT rotor.

Note that performing the inverse design by PROPID code, as a step of the whole optimization procedure, just aims to obtain the blade shape corresponding to a candidate λ_{dgn}. Then, P_{favg} for each candidate rotor obtained by the Bladed-based dynamic simulation can reflect the flow dynamics predicted by the aeroelastic code. Moreover, the maximum P_{favg} corresponds to an appropriate coordination between the static aerodynamic performance and MPPT dynamics.

4. Simulation Results

The inverse design method and the proposed one are respectively applied to optimize the aerodynamic shape of the baseline rotor. Comparison and analysis are conducted to verify the effectiveness of the joint optimization.

4.1. Baseline Wind Turbine and the Parameters of Turbulent Wind

The 1.5 MW WindPACT turbine [37] is chosen as the baseline and its blade geometry is listed in Table 2.

Table 2. Geometry of the NREL 1.5 MW wind turbine blade.

Element	Position (m)	Chord (m)	Twist (°)	Airfoil
1	1.75	1.95	11.10	
2	2.86	1.95	11.10	cylinder
3	5.08	2.27	11.10	
4	7.30	2.59	11.10	
5	9.51	2.74	10.41	
6	11.73	2.58	8.38	s818
7	13.95	2.41	6.35	
8	16.16	2.25	4.33	
9	18.38	2.08	2.85	
10	20.60	1.92	2.22	
11	22.81	1.75	1.58	s825
12	25.03	1.59	0.95	
13	27.25	1.43	0.53	
14	29.46	1.28	0.38	
15	31.68	1.13	0.23	
16	33.90	0.98	0.08	s826
17	35.00	0.50	0.00	

The parameters for the Bladed software to generate a three-dimensional turbulent wind are summarized in Table 3. They are determined in compliance with the IEC61400-1 regulation [39]. Note that in order to represent the common turbulence characteristic of a wind farm, this turbulent wind should be generated according to the specified mean wind speed and turbulence intensity, which can be statistically determined by long-term wind data of a wind farm. To highlight the comprehensive impact of λ_{dgn} on wind energy production, the simulation case aims at low wind speed regions (such as the southeast of China [41,42]). Furthermore, by referring to the specifications of the commercial wind turbines manufactured by Envision Energy [43] (see Table 4), the mean wind speed of turbulence is set to 6.5 m/s. Therefore, the wind turbine rotor optimized by the proposed method is suitable for low wind speed VSWTs.

Table 3. Parameters for generating 3D turbulent wind.

Parameters	Value	Unit
Mean wind speed	6.5	m/s
Height at which speed is defined	84	m
Number of grid points in the lateral direction	30	-
Number of grid points in the vertical direction	30	-
Grid width	150	m
Grid height	150	m
Nyquist frequency of turbulent wind field	27.7031	Hz
Time series length	3600	s
Time step	0.05	s
Turbulence model	IEC Kaimal	-
Turbulence class	A	-

Table 4. Specifications of the low wind speed wind turbines developed by Envision Energy.

Turbine Type	1.5-93	1.8-106	2.2-115	2.2-121
IEC class	IEC S	IEC S	IEC S	IEC S
Design mean wind speed (m/s)	6.5	6	6.5	6.5
Rotor diameter (m)	93	106	115	121
Cut-in wind speed (m/s)	3	3	3	3
Rated power (kW)	1500	1800	2200	2200
Rated wind speed (m/s)	9.5	9.5	9	9
Cut-out wind speed (m/s)	20	25	20	20

4.2. Determination of λ_{dgn} for the Inverse Design Method

As mentioned above, λ_{dgn} and the aerodynamic shape are separately obtained in the conventional inverse design method. Moreover, the primary aim of these methods is usually to improve $C_{p,max}$ at λ_{dgn} [11–16] based on the implicit assumption that VSWTs can be maintained at λ_{dgn} by the MPPT controller. Therefore, λ_{dgn} that can contribute to the increasing of $C_{p,max}$ is of high priority.

To the authors' knowledge, λ_{dgn} is commonly determined based on the empirical analysis [14,15]. Furthermore, λ_{dgn} corresponding to the maximum $C_{p,max}$ is selected according to the functional relation between λ_{dgn} and $C_{p,max}$, which, however, is derived based on single-airfoil wind turbine rotors [24–27]. Because it is hard to deduce the analytical relationship between λ_{dgn} and $C_{p,max}$ for multi-airfoil wind turbine rotors, in implementing the inverse design method in this paper, λ_{dgn} is chosen as 8.5 according to the analysis result presented in Section 2.1.

4.3. Performance Comparison of the Optimized Wind Turbine Rotors

The optimized wind turbine rotors obtained by the inverse design method (hereinafter referred to as "separately-optimized rotor") and the proposed method (hereinafter referred to as "jointly-optimized rotor") are compared from the following aspects.

4.3.1. Aerodynamic Shape

The distributions of chord length and twist angle for the optimized and the original wind turbine rotors are respectively plotted in Figure 8. It can be observed from Figure 8a that compared to the original rotor, the chord length of the jointly-optimized rotor is averagely increased by 16.5%, while the chord length of the separately-optimized rotor is obviously decreased for the most part of the blade except the segments near blade root. As shown in Figure 8b, the twist angle of the jointly-optimized rotor is larger than the original rotor at the segments near the blade root and tip, while the twist angle of the separately-optimized rotor is reduced near the root and increased near the tip.
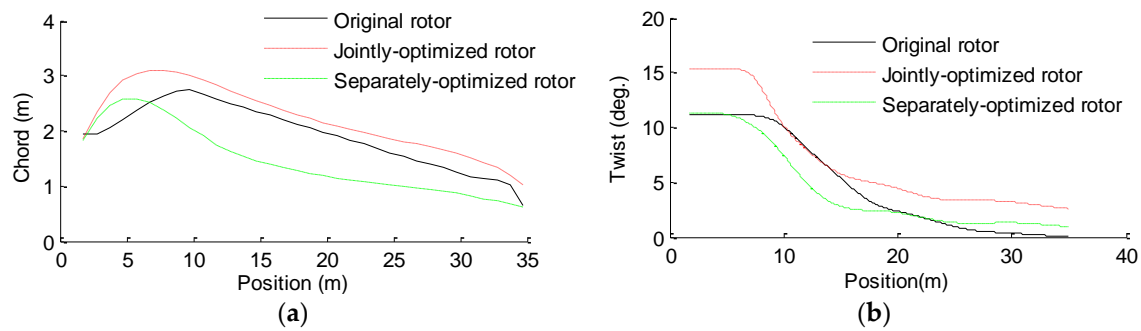
Figure 8. Distributions of chord length and twist angle for the original and optimized blades. (**a**) Chord length; (**b**) Twist angle.

It is important to note that to highlight the effect of λ_{dgn} on the closed-loop performance of VSWTs through the dynamic process of MPPT, some constraints on rotor loads and material cost are not included in this paper, which results in a relatively large adjustment of aerodynamic shape. Therefore, to improve the applicability of the proposed work, the joint aerodynamic optimization considering the above constraints is worth developing further in the future.

4.3.2. Power Coefficient versus TSR Curve (Static Aerodynamic Performance)

The power coefficient C_p versus TSR curves of the optimized wind turbine rotors are compared in Figure 9. Although the shapes of the two curves are very similar, the optimal TSR, namely λ_{dgn}, of the separately-optimized rotor (which equals to 8.5) is notably larger than that of the jointly-optimized rotor (which equals to 6.4) and $C_{p,max}$ of the former rotor is 0.97% greater than for the latter rotor, which is consistent with the analysis in Section 2.1.
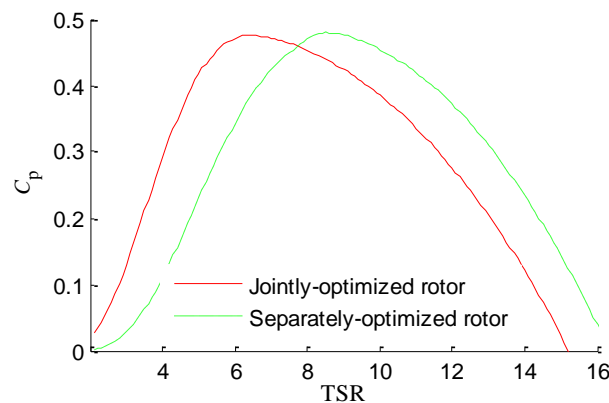

Figure 9. Power coefficient versus TSR curves of the optimized rotors.

4.3.3. Probability Distribution of Operational TSR (MPPT Dynamics)

By comparing the probability distribution of the operational TSR corresponding to the two optimized rotors, as shown in Figure 10, the jointly-optimized rotor operates around the optimal TSR more frequently, which agrees with the analysis in Section 2.2.
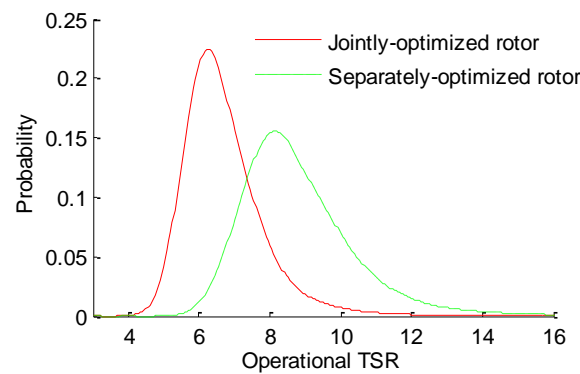
Figure 10. Probability distribution of operating TSR of the optimized rotors.

4.3.4. Closed-Loop Performance

The static and closed-loop performance of the optimized wind turbine rotors are summarized in Table 5. To estimate the dynamic annual energy production (AEP) [5], the dynamic simulation on the closed-loop VSWT system is firstly conducted for a different turbulent wind with a different mean wind speed from the cut-in (3 m/s) to cut-out limit (25 m/s), and the wind power generation corresponding to a different mean wind speed is then weighted with the given Weibull probability density function of wind speed. The shape and scale parameters in the probability density function are set to 1.97 and 7.35 [42].

Table 5. Comparison results of the static and closed-loop performance between different rotors.

Rotor	Separately-Optimized	Jointly-Optimized
λ_{dgn}	8.5	6.4
$C_{p,max}$	0.4790 (+0.97%)	0.4744
P_{favg}	0.4452	0.4575 (+2.76%)
Dynamic AEP (MWh)	3985.89	4233.65 (+6.21%)

It is revealed from Table 5 that although $C_{p,max}$ of the separately-optimized rotor is 0.97% larger than that of the jointly-optimized one, the latter rotor can capture 2.76% more wind energy from the turbulence (mean wind speed is 6.5 m/s) and correspondingly the increase in annual energy yield is 247.76 MWh (6.21%). This indicates that shortening the tracking range and increasing the frequency of the wind turbine rotor operating around the optimal TSR by decreasing λ_{dgn} can improve wind energy production more effectively than increasing $C_{p,max}$. In other words, the MPPT dynamics play a more prominent role in the closed-loop performance than the static aerodynamic performance. Through the coordination between the static aerodynamic performance and the MPPT dynamics performed by the proposed method, higher wind energy capture efficiency of VSWTs under turbulence can be achieved.

5. Conclusions

This paper firstly reveals that λ_{dgn} exerts a comprehensive influence upon the overall efficiency of the closed-loop VSWT system through static aerodynamic performance and the dynamic process of MPPT. With the increase of λ_{dgn}, though $C_{p,max}$ is improved, the tracking range of rotor speed as well as the dynamic process of MPPT become longer, which might eventually reduce the wind energy capture efficiency. Therefore, in the inverse aerodynamic design for VSWTs, the impact of λ_{dgn} on the static performance and the MPPT dynamic process should be compromised for determining an appropriate λ_{dgn}.

Based on the inverse design program PROPID for the aerodynamic optimization of VSWTs, this paper then proposes a new method, fully considering the impact of λ_{dgn} on the static and dynamic

behavior of wind turbines. Different from the conventional separated design procedure, the design TSR, chord length and twist angle are jointly optimized to maximize the closed-loop performance of VSWTs, namely wind energy capture efficiency, in this method. Through the coordination between the static aerodynamic performance and the MPPT dynamics performed by the proposed method, higher wind energy capture efficiency of VSWTs under turbulence can be achieved, which is validated by the simulation results based on the Bladed software.

Author Contributions: Minghui Yin and Yun Zou proposed the motivation and improvement idea of the optimization strategy; Zhiqiang Yang built the optimization model and performed the numerical experiments; Yan Xu and Zhao Yang Dong provided guidance and key suggestions; Zhiqiang Yang, Minghui Yin, Yan Xu, Yun Zou, Zhao Yang Dong and Qian Zhou wrote the paper.

Conflicts of Interest: The authors declare no conflict of interest.

Appendix A. Lift Coefficient and Axial Induction Factor Distributions

The lift coefficient C_L and axial induction factor a of each blade section used in the input file of PROPID code are listed in Table A1.

Table A1. Lift coefficient and axial induction factor distributions.

r/R	C_L	a
0.05	0	0
0.15	1.25	0.183
0.25	1.60	0.283
0.35	1.45	0.333
0.45	1.35	0.333
0.55	1.30	0.333
0.65	1.25	0.333
0.75	1.15	0.333
0.85	1.12	0.333
0.95	1.09	0.333

References

1. Schubel, P.J.; Crossley, R.J. Wind turbine blade design. *Energies* **2012**, *5*, 3425–3449. [CrossRef]
2. Fuglsang, P.; Madsen, H.A. Optimization method for wind turbine rotors. *J. Wind Eng. Ind. Aerodyn.* **1999**, *80*, 191–206. [CrossRef]
3. Benini, E.; Toffolo, A. Optimal design of horizontal-axis wind turbines using blade-element theory and evolutionary computation. *J. Sol. Energy Eng.* **2002**, *124*, 357–363. [CrossRef]
4. Wang, X.; Shen, W.Z.; Zhu, W.J.; Sørensen, J.N.; Jin, C. Shape optimization of wind turbine blades. *Wind Energy* **2009**, *12*, 781–803.
5. Bottasso, C.L.; Campagnolo, F.; Croce, A. Multi-disciplinary constrained optimization of wind turbines. *Multibody Syst. Dyn.* **2012**, *27*, 21–53. [CrossRef]
6. Tahani, M.; Babayan, N.; Mehrnia, S.; Shadmehri, M. A novel heuristic method for optimization of straight blade vertical axis wind turbine. *Energy Convers. Manag.* **2016**, *127*, 461–476. [CrossRef]
7. Campobasso, M.S.; Minisci, E.; Caboni, M. Aerodynamic design optimization of wind turbine rotors under geometric uncertainty. *Wind Energy* **2016**, *19*, 51–65. [CrossRef]
8. Sessarego, M.; Ramos-García, N.; Yang, H.; Shen, W.Z. Aerodynamic wind-turbine rotor design using surrogate modeling and three-dimensional viscous-inviscid interaction technique. *Renew. Energy* **2016**, *93*, 620–635. [CrossRef]

9.　Pourrajabian, A.; Afshar, P.A.N.; Ahmadizadeh, M.; Wood, D. Aero-structural design and optimization of a small wind turbine blade. *Renew. Energy* **2016**, *87*, 837–848. [CrossRef]

10.　Yang, Z.; Yin, M.; Xu, Y.; Zhang, Z.; Zou, Y.; Dong, Z.Y. A multi-point method considering the maximum power point tracking dynamic process for aerodynamic optimization of variable-speed wind turbine blades. *Energies* **2016**, *9*. [CrossRef]

11.　Glauert, H. *Airplane Propellers*; Springer: Berlin/Heidelberg, Germany, 1935.

12.　Wilson, R.E.; Lissaman, P.B.; Walker, S.N. *Aerodynamic Performance of Wind Turbines*; Oregon State University: Corvallis, OR, USA, 1976.

13.　Sedaghat, A.; Mirhosseini, M. Aerodynamic design of a 300 kW horizontal axis wind turbine for province of Semnan. *Energy Convers. Manag.* **2012**, *63*, 87–94. [CrossRef]

14.　Kim, B.; Kim, W.; Bae, S.; Park, J.; Kim, M. Aerodynamic design and performance analysis of multi-MW class wind turbine blade. *J. Mech. Sci. Technol.* **2011**, *25*, 1995–2002. [CrossRef]

15.　Johansen, J.; Madsen, H.A.; Gaunaa, M.; Bak, C.; Sørensen, N.N. Design of a wind turbine rotor for maximum aerodynamic efficiency. *Wind Energy* **2009**, *12*, 261–273. [CrossRef]

16.　Scappatici, L.; Bartolini, N.; Castellani, F.; Astolfi, D.; Garinei, A.; Pennicchi, M. Optimizing the design of horizontal-axis small wind turbines: From the laboratory to market. *J. Wind Eng. Ind. Aerodyn.* **2016**, *154*, 58–68. [CrossRef]

17.　Sørensen, J.N.; Okulov, V.L.; Mikkelsen, R.F.; Naumov, I.V.; Litvinov, I.V. Comparison of classical methods for blade design and the influence of tip correction on rotor performance. *J. Phys. Conf. Ser.* **2016**, *753*. [CrossRef]

18.　Eminoglu, U.; Ayasun, S. Modeling and design optimization of variable-speed wind turbine systems. *Energies* **2014**, *7*, 402–419. [CrossRef]

19.　Cheng, M.; Zhu, Y. The state of the art of wind energy conversion systems and technologies: A review. *Energy Convers. Manag.* **2014**, *88*, 332–347. [CrossRef]

20.　Johnson, K.E.; Fingersh, L.J.; Balas, M.J.; Pao, L.Y. Methods for increasing region 2 power capture on a variable-speed wind turbine. *J. Sol. Energy Eng.* **2004**, *126*, 1092–1100. [CrossRef]

21.　Kim, Y.S.; Chung, I.Y.; Moon, S.I. An analysis of variable-speed wind turbine power-control methods with fluctuating wind speed. *Energies* **2013**, *6*, 3323–3338. [CrossRef]

22.　Ragheb, M.; Ragheb, A.M. *Wind Turbines Theory—The Betz Equation and Optimal Rotor Tip Speed Ratio*; InTech: Vienna, Austria, 2011.

23.　Bak, C. Sensitivity of key parameters in aerodynamic wind turbine rotor design on power and energy performance. *J. Phys. Conf. Ser.* **2007**, *75*. [CrossRef]

24.　Yurdusev, M.A.; Ata, R.; Çetin, N.S. Assessment of optimum tip speed ratio in wind turbines using artificial neural networks. *Energy* **2006**, *31*, 2153–2161. [CrossRef]

25.　Ata, R.; Kocyigit, Y. An adaptive neuro-fuzzy inference system approach for prediction of tip speed ratio in wind turbines. *Expert Syst. Appl.* **2010**, *37*, 5454–5460. [CrossRef]

26.　Çetin, N.S.; Yurdusev, M.A.; Ata, R.; Özdamar, A. Assessment of optimum tip speed ratio of wind turbines. *Math. Comput. Appl.* **2005**, *10*, 147–154. [CrossRef]

27.　Manwell, J.F.; McGowan, J.G.; Rogers, A.L. *Wind Energy Explained: Theory, Design and Application*; John Wiley & Sons: New York, NY, USA, 2010.

28.　Bossanyi, E.A. Wind turbine control for load reduction. *Wind Energy* **2003**, *6*, 229–244. [CrossRef]

29.　Bossanyi, E.A. The design of closed loop controllers for wind turbines. *Wind Energy* **2000**, *3*, 149–163. [CrossRef]

30.　Tang, C.; Soong, W.L.; Freere, P.; Pathmanathan, M.; Ertugrul, N. Dynamic wind turbine output power reduction under varying wind speed conditions due to inertia. *Wind Energy* **2013**, *16*, 561–573. [CrossRef]

31.　Morren, J.; Pierik, J.; de Haan, S.W. Inertial response of variable speed wind turbines. *Electr. Power Syst. Res.* **2006**, *76*, 980–987. [CrossRef]

32.　Zhang, X.; Yin, M.; Zhou, L.; Zou, Y.; Chen, Z. Analysis on factors affecting performance of MPPT control. *Autom. Electr. Power Syst.* **2013**, *37*, 15–21.

33.　Griffin, D.A. *NREL Advanced Research Turbine (ART) Aerodynamic Design of ART-2B Rotor Blades*; Office of Scientific & Technical Information Technical Reports; National Renewable Energy Laboratory (NREL): Golden, CO, USA, 2000.

34.　Seling, M.S. *PROPID User Manual*; Version 5.3.1; UIUC Applied Aerodynamics Group: Champaign, IL, USA, 2012.

35. Bossanyi, E.A. *GH Bladed Theory Manual*; GH & Partners Ltd.: New York, NY, USA, 2003.

36. Kim, B.; Kim, W.; Lee, S.; Bae, S.; Lee, Y. Developement and verification of a performance based optimal design software for wind turbine blades. *Renew. Energy* **2013**, *54*, 166–172. [CrossRef]

37. Malcolm, D.J.; Hansen, A.C. *WindPACT Turbine Rotor Design Study*; National Renewable Energy Laboratory: Golden, CO, USA, 2002.

38. Abdullah, M.A.; Yatim, A.H.M.; Tan, C.W.; Saidur, R. A review of maximum power point tracking algorithms for wind energy systems. *Renew. Sustain. Energy Rev.* **2012**, *16*, 3220–3227. [CrossRef]

39. *Wind Turbine—Part 1: Design Requirements*; IEC 61400-1; International Electrotechnical Commission: Geneva, Switzerland, 2005.

40. Wang, H.; Zhang, R.; Liu, W.; Wang, G.; Gin, B. Improved interpolation method based on singular spectrum analysis iteration and its application to missing data recovery. *Appl. Math. Mech.* **2008**, *29*, 1351–1361. [CrossRef]

41. Zhang, J.; Zhou, Z.; Lei, Y. Design and research of high-performance low-speed wind turbine blades. In Proceedings of the 2009 World Non-Grid-Connected Wind Power and Energy Conference, Nanjing, China, 24–26 September 2009.

42. Zhou, W.; Yang, H.; Fang, Z. Wind power potential and characteristic analysis of the Pearl River Delta region, China. *Renew. Energy* **2006**, *31*, 739–753. [CrossRef]

43. Smart On-Shore Wind Turbine. Available online: http://www.envisioncn.com/pdf/lushang.pdf (accessed on 22 November 2016).